Journal of Fluorine Chemistry 134 (2012) 44–48

Contents lists available at ScienceDirect

Journal of Fluorine Chemistry

journal homepage: www.elsevier.com/locate/fluor

Structural effects on the electrical conductivity of molten fluorides: Comparison between LiF–YF_3 and LiF–NaF–ZrF_4

Anne-Laure Rollet, Mathieu Salanne, Henri Groult *

UPMC Univ Paris 06, CNRS, ESPCI, Laboratoire PECSA, 4 place Jussieu, 75005 Paris, France

ARTICLE INFO

Article history:
Received 30 January 2011
Received in revised form 4 April 2011
Accepted 7 April 2011
Available online 19 April 2011

Keywords:
Molten salt
Molten fluoride
Electrical conductivity
Impedance
Molecular dynamics
Structure

ABSTRACT

The electrical conductivities of molten LiF–YF_3 and LiF–NaF–ZrF_4 have been obtained from impedance measurements and molecular dynamics simulations, and discussed through the analysis of the local structure of the liquid. The conductivity decreases with addition of MF_n (M^{n+} = Y^{3+} or Zr^{4+}) in the melt due to the formation of MF_x^{n-x} units, which can be either isolated or linked via bridging fluorine. Structural differences have been put in evidence depending on the nature of the multivalent metallic species (Y^{3+} and Zr^{4+}) added in the alkali fluoride solvent regarding the stability of the MF_x^{n-x} units and the length m of $[MF_x^{n-x}]_m$ chains. These differences are at the origin of a more pronounced decrease of the electrical conductivity in the Zr-containing fused salts in the low MF_n concentration régime.

Research topic

The laboratory has been involved in fluorine chemistry for more than 50 years mainly in the field of molten fluorides. Our present contribution concerns the energy storage and conversion. In both cases, our scientific approach is to combine experiments and theory in order to propose realistic interpretations of the observed phenomena. Thus, we are deeply involved in the development of the nuclear cycle: one part of our activity is performed in collaboration with Areva-Comurhex via the study of the fluorine production from electrolysis of molten KF–nHF; indeed, F_2 is used as fluorinated agent for the synthesis of uranium hexafluorides which serve to the uranium enrichment. Our attention has been paid not only on the electrochemical process leading to the formation of F_2 and H_2 gases, but also on the electrolyte structure and the electrode/electrolyte interface from simulation. Another part of our activity has been focused on the development of the molten salt reactor for the next generation of nuclear plants (Generation IV) within the frame of the PACEN program (Programme sur l'Aval du Cycle et l'Energie Nucléaire) supported by the Centre National de la Recherche Scientifique (CNRS). In these reactors, the fuel is dissolved in the molten fluorides. Our objectives are to understand the short-range structure of the species involved in the foreseen molten salts, to analyze the influence of the speciation of all the ions on the thermochemical properties, to study the transport of heat and matter which vary a lot from a molten salt to another, to perform the extraction of heavy metals from the fused salts. This is done by running molecular dynamics simulations coupled with experimental investigations by physical-chemical methods such as NMR or EXAFS (through collaborations with CEMHTI-CNRS Orléans) or by electrochemical studies as for the determination of the electrical conductivity. In the field of energy storage, the studies are focussed on the preparation, the characterisation and the study of the electrochemical performances of fluorinated materials used as positive electrodes in non-rechargeable (case of graphite fluorides) or rechargeable (case of FeF_3, CoF_3, etc.) lithium battery. In both cases, the nano-sized fluorinated compounds are investigated.

1. Introduction

Molten fluorides are a particular class of liquids because all the components are ionic. They are very fascinating because depending on the nature of the cations, the liquid structure may switch from a simple bath of charged hard spheres to a liquid network or a liquid with free complexes [1]. In addition to the fundamental aspects, molten fluorides are used in several applications. One may cite the fluorine production [2,3], the aluminium electrolysis [4], the pyrochemical treatment of nuclear waste [5,6], the generation IV nuclear reactors [7,8], the synthesis of materials for lasers, phosphor lamps [9,10] and electrochemical sensors [11]. Rare

* Corresponding author. Tel.: +33 1 44 27 32 65; fax: +33 1 44 27 32 28.
E-mail addresses: anne-laure.rollet@upmc.fr (A.-L. Rollet), henri.groult@upmc.fr, mathieu.salanne@upmc.fr (H. Groult).

0022-1139/$ – see front matter © 2011 Elsevier B.V. All rights reserved.
doi:10.1016/j.jfluchem.2011.04.002

earth fluorides are crucial in the nuclear applications. Rare earths are indeed a product of the nuclear reaction; as soon as they are formed they act as a poison for the chain reaction. Solutions therefore have to be found to remove them from the core. In the case of molten salt reactor (MSR) this operation may be feasible during the running of the reactor because the fuel is at the liquid state and an on-line reprocessing can be performed. Nevertheless, this appealing concept – with important reduction of inventories and induced radiotoxicities at equilibrium compared to other fuel cycles [7] – is still under study. Among the questions to answer remains the physico-chemical behaviour of the salt inside the recycling circuit. The speciation of all the ions greatly influences a lot of thermochemical properties; for example the nature of most species is important in determining the solubility of heavy metals, and especially of actinide cations. Transport of heat and matter also vary a lot from a molten salt to another and it is important to determine precisely these quantities. In liquids, the short-range structure can be probed by many various spectroscopy techniques. In molten fluorides, only Raman [12–14], NMR [15,16] and EXAFS [17–21] studies have been undertaken because of the experimental hindrances (high temperature, high corrosiveness, volatility...). These techniques have been proved to be efficient in giving insight into the cationic environments in a wide range of melt compositions. Matter transport coefficients are still more difficult to quantify with precision because, in addition to the 'usual' experimental difficulties of handling fluorides, the temperature has to be stable, homogeneous and well monitored during the experiments. Very recently, a new setup NMR setup has been developed to measure self-diffusion coefficients in molten fluorides up to 1500 K [22–24].

In this paper, we focus on collective transport coefficients: the electrical conductivities. We combine their experimental and theoretical determination. Although this quantity has commonly been measured in molten chlorides, less data are available in molten fluorides [25]. Indeed, these experiments are very difficult to set up because of the important reactivity of these melts towards oxide glasses. To overcome this difficulty, an electrochemical cell, based on pyrolytic boron nitride, was developed by Hives and Thonstad [26], who successfully used it to measure electrical conductivities of aluminium-based molten fluorides. The theoretical determination is based here on molecular dynamics (MD) simulations using a polarizable ion model (PIM) [27]. In a previous paper [28], we have showed how it is possible to build a polarizable interaction potential for mixtures of LiF, NaF, KF and ZrF_4 from a purely first-principles basis. The accuracy of the simulations was checked by computing heat-transfer properties, like heat capacities, electrical conductivities and viscosities, which compared satisfactorily with experimental measures, for two different salts (LiF–NaF–KF and NaF–ZrF_4 mixtures) [28,29].

In the present paper, the changes in transport properties induced by the addition of yttrium and zirconium fluorides in molten alkali fluoride mixtures have been compared. Yttrium is a model element for small size, trivalent lanthanides while zirconium is often used as a substitute of tetravalent actinides. The electrical conductivities are determined as a function of the yttrium/zirconium content and are complemented by the MD simulations for an interpretation of the results from the structural point of view.

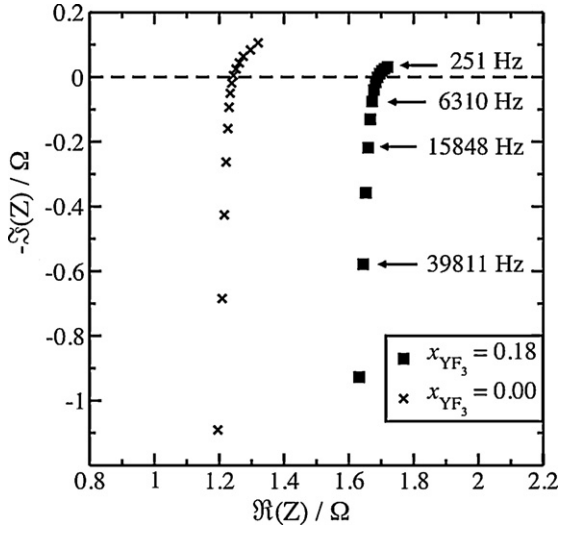

Fig. 1. Experimental impedance spectra recorded for pure LiF and for LiF–YF_3 ($x_{YF_3} = 0.18$) at $T = 1133$ K.

2. Results and discussion

Impedance experiments were carried out for LiF–YF_3 and LiF–NaF–ZrF_4 mixtures with different concentrations of YF_3 and ZrF_4. The experimental impedance spectra recorded for pure LiF and for LiF–YF_3 ($x_{YF_3} = 0.18$) at $T = 1133$ K are presented in Fig. 1.

The intercept of the curve with the real axis gives rise to the electrolyte resistance from which the electrical conductivity (χ) values are deduced. Such impedance spectra have been recorded at $T = 1133$ K for LiF–YF_3 for compositions ranging from $x_{YF_3} = 0$ up to the eutectic composition $x_{YF_3} = 0.18$, and at several temperatures between 900 K and 1073 K for LiF–NaF–ZrF_4 for $x_{ZrF_4} \in [0; 0.29]$ (in that case the NaF/LiF ratio was kept constant, with 61% of LiF and 39% of NaF).

In molecular dynamics simulations, the electrical conductivity is calculated from

$$\chi = \frac{e^2}{k_B T V} \lim_{t \to \infty} \frac{1}{6t} \left\langle \left| \sum_{\alpha}^{N_\alpha} q_\alpha \Delta_\alpha(t) \right|^2 \right\rangle$$

where k_B is Boltzmann's constant, T the temperature, V the volume of the simulation cell, and $\Delta_\alpha(t) = \sum_{i \in \alpha} \delta r_i(t)$ is the net displacement of all the ions of species α in time t. Note that the electrical conductivity being a collective quantity, its computation requires long simulation times; the values calculated here have error bars of the order of 10%. Here the use of the Nernst–Einstein equation, which relates the electrical conductivity to the individual diffusion coefficients of the various species, would lead to unrealistically high values: It is essential to take into account the correlations between the zirconium and the fluoride ions.

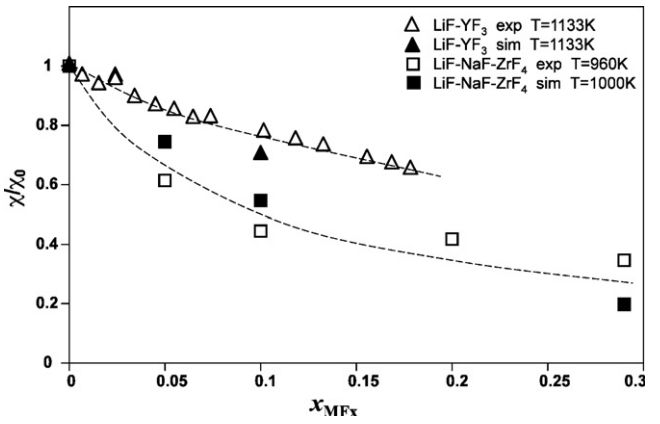

Fig. 2. Variation of the reduced conductivity χ/χ_0 versus the molar fraction of MF_n, where χ_0 is the conductivity for the corresponding molten alkali fluoride solvent ($x_{MF_n} = 0$).

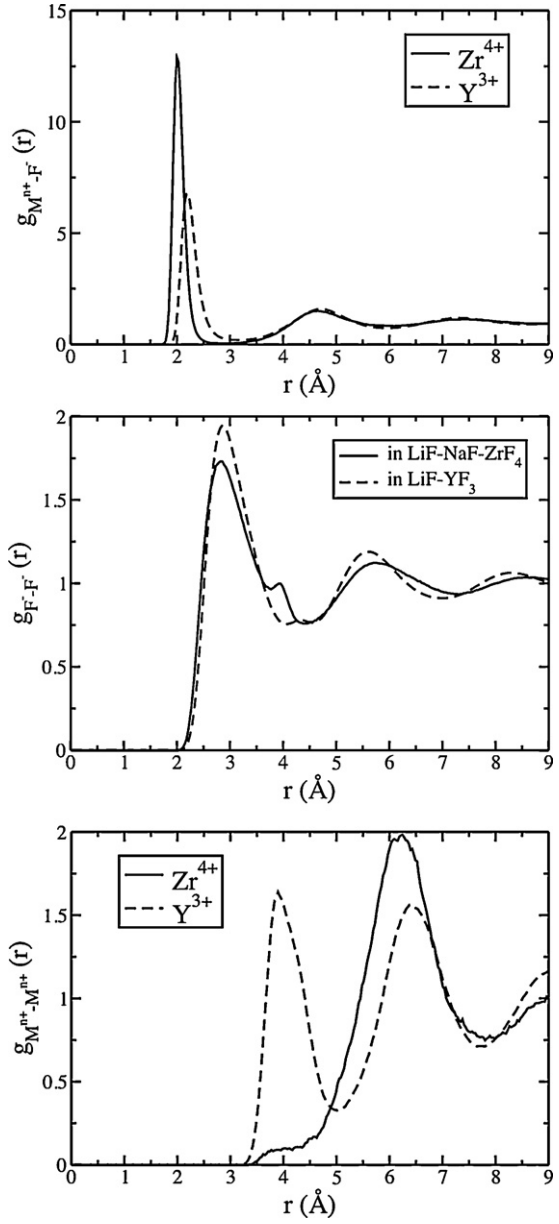

Fig. 3. Radial distribution functions $g_{MF}(r)$ (top), $g_{FF}(r)$ (middle) and $g_{MM}(r)$ (bottom) for LiF–YF_3 at $x_{YF_3} = 0.1$ (T = 1133 K) and for LiF–NaF–ZrF_4 at $x_{ZrF_4} = 0.1$ (T = 1000 K).

In order to facilitate the comparison between both systems, we have defined in this work a reduced electrical conductivity value, χ/χ_0, where χ_0 is the electrical conductivity of the pure alkali fluoride solvent (i.e. LiF or LiF–NaF) without any additive. To this end, we used electrical conductivities of the LiF–NaF eutectic mixture and of LiF that have been reported in Ref. [25]. The use of this reduced function also allows us to focus on the composition effect only: The temperature effects on χ and χ_0 cancel one with each other. The quantity χ/χ_0 is plotted in Fig. 2 versus the molar fraction in MF_x (where $M^{x+} = Y^{3+}$ or Zr^{4+}) in order to compare the respective influence of the two cations. Whatever the system, a good agreement is observed between the calculated and the experimental values. In the case of the zirconium-based system, this is not surprising since the accuracy of the model was proved by reproducing the structural data in LiF–ZrF_4 over a wide range of compositions [30]. Nevertheless, agreement of simulations with transport data is a severe test of their accuracy.

In both systems, χ/χ_0 decreases monotonously when MF_x is added. However, the variation differs between ZrF_4 and YF_3. On the one hand, for YF_3, χ/χ_0 decreases almost linearly with x_{YF_3} in the range of concentration investigated. On the other hand for ZrF_4, χ/χ_0 decreases strongly at low ZrF_4 amounts ($x_{ZrF_4} < 0.1$) and more slowly afterwards.

In order to analyze these different behaviors, we consider the local structure around the two species M^{x+} and their evolution with x_{MF_x}, which also exhibit some differences. To this end, we have plotted in Fig. 3 the radial distribution functions (RDF) $g_{MF}(r)$ and $g_{MM}(r)$ in the two systems, for the same value of 0.1 for x_{MF_x}, as calculated during the MD simulations. Note that the temperatures are different, but we did not observe noticeable changes of the RDF with temperature in such systems.

In particular, the $g_{MF}(r)$ provides the information on how the metallic ion is solvated in the alkali fluoride bath. Here the first peak stands at a shorter distance in the zirconium-containing system than in the yttrium-containing one. Moreover, this first peak is much more intense, with a smaller width, in the LiF–NaF–ZrF_4 systems. The maximum of the first peak is related to the association between the cations and the anions. Ergo, the association between fluorine and zirconium is much stronger than between fluorine and yttrium. The repulsion terms, which are modelled by a Buckingham-type potential, have some very similar shapes for the two cations (which is to be expected because they are isoelectronic), so that this effect is due to differences between the cation charges only. At low x_{YF_3} (0.10), we observed in the MD simulation that the yttrium can be 6-fold, 7-fold or 8-fold coordinated, with some relative proportions of 15%, 53% and 32%, which is in agreement with previous NMR observations [31]. The observed coordination number value contrasts with the corresponding chloride systems, in which the yttrium is in an octahedral symmetry at low x_{YCl_3} that becomes distorted when x_{YCl_3} is increased [32]. The difference in coordination number can easily be understood in terms of size: The fluoride ions being smaller, more anions are allowed to enter in the yttrium solvation shell. This leads to the structure around yttrium being less symmetrical. The coordination number does not vary monotonously with x_{ZrF_4} in mixtures of alkali fluorides with ZrF_4 [30]. In mixtures of LiF–ZrF_4 with relatively low ZrF_4 amount ($0 < x_{ZrF_4} < 0.15 - 0.2$), it is equal to 7 on average, then it decreases up to 6.4 at $x_{ZrF_4} = 0.35$ before increasing again for $x_{ZrF_4} > 0.35$. The average distance Zr–F follows a similar trend. A tentative explanation of the χ/χ_0 different variations at low amount of MF_x can be the following: although both cations are on average surrounded by 7 fluoride anions the solvation shell is much more structured in the case of zirconium, and the residence time for F^- anions is longer. This leads to a stronger decrease of χ/χ_0 ratio for the LiF–NaF–ZrF_4 system compared to the LiF–YF_3 one.

As soon as x_{MF_n} is increased, in both systems the coordination polyhedra units start to share some fluoride ions, thus forming network liquids [33,32]. In $ZrCl_4$ and $ThCl_4$-based systems, it has been suggested from Raman spectroscopy experiments that the ends of such chains carry lower coordinate cations [34,35]. The most striking evidence of the difference between the two liquid structures is given by the $g_{MM}(r)$. In LiF–YF_3, $g_{MM}(r)$ oscillates regularly from the first Y–Y distance up to several Y–Y shells. It indicates strong correlation between yttrium and regular organization of the yttrium cations in the liquids. This result supports the view of relatively long $[YF_x^{3-x}]_n$ chains. In contrast, in zirconium fluorides, the $g_{MM}(r)$ exhibits tormented feature, with the presence of a small shoulder before the first Zr–Zr first peak. The overall shape of the $g_{MM}(r)$ is typical of much smaller ordering effects than in the YF_3 case: The oscillations seem to be damped rapidly. It was shown that the shoulder corresponds to the fraction of Zr^{4+} ions which are connected via an F^- bridge [30]. Ergo, the chains of

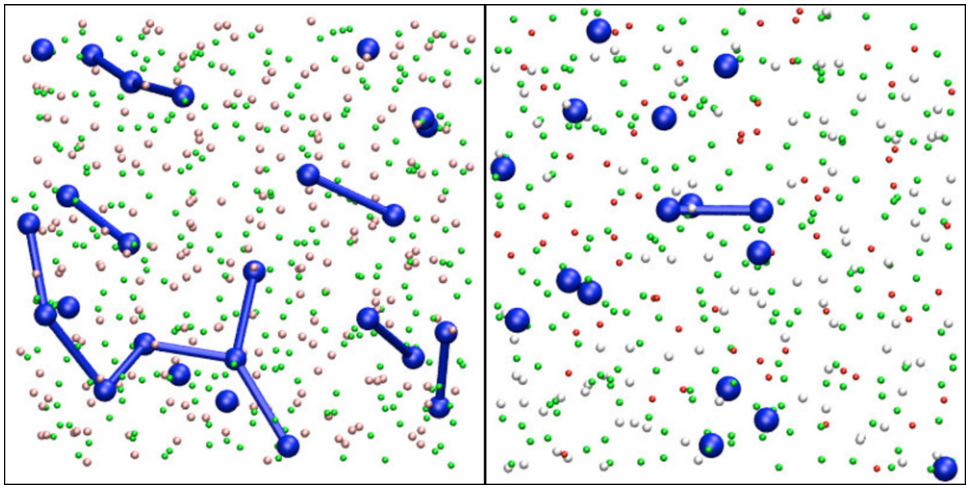

Fig. 4. Snapshots for LiF–YF_3 at $x_{YF_3} = 0.1$ (T = 1133 K) (left) and for LiF–NaF–ZrF_4 at $x_{ZrF_4} = 0.1$ (T = 1000 K) (right). The ions are coloured as follows: Y^{3+} or Zr^{4+} (royal blue), F^- (green), Li^+ (red) and Na^+ (white). The blue line between Y^{3+} or Zr^{4+} ions indicate that they are at a shorter distance than a given cut-off distance. The latter was set to the first minimum of the Y^{3+}–Y^{3+} RDF for LiF–YF_3 and just after the shoulder of the Zr^{4+}–Zr^{4+} RDF in LiF–NaF–ZrF_4. (For interpretation of the references to colour in this figure legend, the reader is referred to the web version of the article.)

$[ZrF_x^{4-x}]_n$ are much shorter than in yttrium fluorides. To illustrate the different structural behaviors between yttrium and zirconium fluoride systems, snapshots of both systems are provided in Fig. 4. They clearly show that $[MF_x^{3-x}]_n$ chains are formed at low MF_n content already ($x_{MF_n} = 0.1$ in this snapshot) in yttrium fluorides and that their length can be relatively long. In zirconium fluorides at the same concentration, there are almost no $[MF_x^{3-x}]_n$ chains.

As such, the structure of the liquids would seem to indicate a more important decrease of the electrical conductivity with composition in LiF–YF_3 due to the network formation. In fact this view is not supported by the data shown in Fig. 2, where one can see that the χ/χ_0 ratio varies in a similar way in the two systems for high values of x_{MF_n}. It should therefore be noted, however, that the snapshots give access to instantaneous information only. In fact, the smaller association between Y^{3+} and F^- than between Zr^{4+} and F^-, which was observed in the corresponding RDFs, is at the origin of a rapid breakdown of the chains formed: The network formed is more labile in LiF–YF_3. Its formation therefore does not influence much the electrical conductivity.

3. Experiments

LiF, NaF, KF, YF_3 and ZrF_4 powders provided by (Sigma–Aldrich) were treated under fluorine atmosphere to remove traces of oxides or hydroxides and stored in a glove box (water content less than 5 ppm) under Ar atmosphere. The constituents of the salt mixtures were mixed, put in a vitreous carbon (about 150 g of salt) which is placed in a vertical furnace and dried before each experiment under vacuum at first at 150 °C for 12 h, and then at 250 °C, 350 °C, 450 °C and 550 °C for 2 h for each temperature step. Then, the cell was put under argon stream and the temperature was increased up to the measurement temperature. For the LiF–YF_3 mixtures all the measurements were performed at 1133 K. For the LiF–NaF–ZrF_4 mixtures the measurements were performed at several temperatures between 900 K and 1073 K. All measurements were performed under argon atmosphere and the temperature of the molten salt was controlled using a chromel–alumel thermocouple. The YF_3 and ZrF_4 concentrations are ranged by introduction of pellets.

Table 1
Parameters of the interaction potential concerning the Y^{3+} ion (atomic units). The polarizability of Y^{3+} was set to 3.8 au. Parameters for the other ions, together with the force field analytic expression, are given in Ref. [28].

Ion pair ij	B^{ij}	a^{ij}	C_6^{ij}	C_8^{ij}	b^{ij}	b_d^{ij}	c^{ij}	c^{ji}
F^-–Y^{3+}	87.4	1.832	0.0	0.0	1.9	1.847	1.966	−0.89
Y^{3+}–Y^{3+}	1.0	5.0	0.0	0.0	1.9	1.0	0.0	0.0
Li^+–Y^{3+}	1.0	5.0	0.0	0.0	1.9	1.0	0.0	0.0

The conductivity cell configuration was derived from the one proposed by Hives and Thonstad [26]. Briefly, the cell consists of a pyrolytic boron nitride tube (inner diameter of 5.9 mm and length of 90 mm) in which an inconel rod electrode (ϕ = 3 mm) which acts as first electrode was introduced and placed in a fixed position. Small holes were performed at the top of the boron nitride tube to remove gas bubbles which could modify the contact between the salt and the inconel electrode. The second electrode was constituted by the glassy carbon crucible itself. After melting, the conductivity cell was immersed into the fused salt. The electrolyte resistance, from which the electrical conductivity value is deduced, was measured by impedance measurements using a Solartron 1260 impedancemeter. The spectra were recorded at free potential (i.e. at open circuit voltage (OCV)). The ac amplitude of the signal was 10 mV and the frequency range was comprised between 100 kHz and 10 Hz. The cell constant (≈13 cm^{-1}) was determined by making the calibration of the cell using LiCl–KCl eutectic mixture (58.8–41.2 mol%) in the temperature range comprised between 690 K and 890 K and using LiF between 1123 K and 1223 K.

We have used a molecular dynamics (MD) code in which the polarisable ion model is implemented. This code is dedicated to calculations in ionic liquids [36]. It allows us to generate via classical molecular dynamics calculations the trajectories of ions inside a periodically replicated simulation cell and then to extract the relevant physicochemical properties of the melt. The interaction potential consists of a sum of pairwise additive interactions supplemented with a many-body polarization term, as previously described by Salanne et al. [37,28]. The various parameters involved in the interaction potential were constructed through a "force-fitting" procedure. To determine forces and dipoles of each ions, first-principles electronic structure calculations are performed for a given system using the plane waves density functional theory formalism. Parameters of the potential are then obtained by minimizing the difference between the forces and the dipoles predicted by the model to the first-principles calculated ones. The parameters involving the F^-, Li^+, Na^+ and Zr^{4+} are listed in Ref. [28]; the ones involving the Y^{3+} ion are given in Table 1.

MD simulations were then carried out on molten LiF–NaF–ZrF_4 and LiF–YF_3 mixtures. Calculations were performed at 1000 K for LiF–NaF–ZrF_4 and at 1133 K for LiF–YF_3. In each case, the systems were first equilibrated in the NPT ensemble with a pressure fixed to 0 GPa. Second, NVT ensemble runs were realized at the equilibrated cell volume. The method used to enforce NVT ensemble sampling is the Nosé–Hoover chain thermostat method [38,39]. The total simulation times were of 2 ns, with a time step of 0.5 fs.

4. Conclusions

In conclusion we have shown in this paper that the electrical conductivity changes upon addition of multivalent metallic species (Y^{3+} and Zr^{4+}) in an alkali fluoride solvent can be interpreted in terms of structural features. The electrical conductivities were evaluated from both impedance spectra measurements and molecular dynamics simulations. Both sets of data agreed well one with each other. In order to quantify the effect of the M^{n+} ions, the results were analyzed using a reduced χ/χ_0 ratio. In both cases, this quantity decreases due to the formation of solvated metal ion complexes. These complexes were identified in the molecular dynamics simulations, and the M^{n+}–F^- interaction was shown to play an important role in the electrical conductivity drop. Because of their higher charge, zirconium ions form more stable complexes, preventing part of the ions to participate to the electrical current conduction. Finally, we could show that YF_x units have a greater tendency to form longer chains bond by bridging fluoride anions.

Acknowledgements

The authors would like to acknowledge the financial support of PACEN (Programme sur l'Aval du Cycle et l'Energie Nucléaire) through PCR-RSF and GDR PARIS programmes. Pr. D. Avignant (UBP, Clermont-Ferrand) is gratefully acknowledged for his help in salt purification. They thank also José Gomez (UPMC, Paris) for the electrode preparation.

References

[1] A.-L. Rollet, M. Salanne, Annu. Rep. Prog. Chem., Sect. C, doi:10.1039/c1pc90003j.
[2] H. Groult, C. Simon, A. Mantoux, F. Lantelme, P. Turq, in: T. Nakajima, H. Groult (Eds.), Fluorinated Materials for Energy Conversion, Elsevier, 2005, pp. 1–29.
[3] H. Groult, F. Lantelme, M. Salanne, C. Simon, C. Belhomme, B. Morel, F. Nicolas, J. Fluorine Chem. 128 (2007) 285–295.
[4] K. Grojtheim, C. Krohn, M. Malinovsky, K. Matiasovsky, J. Thonstad, Aluminium Electrolysis Fundamentals of the Hall–Heroult Process, 2nd ed., Aluminium-Verlag, Düsseldorf, 1982.
[5] P. Taxil, L. Massot, C. Nourry, M. Gibilaro, P. Chamelot, L. Cassayre, J. Fluorine Chem. 130 (2009) 94–101.
[6] P. Chamelot, L. Massot, L. Cassayre, P. Taxil, Electrochim. Acta 55 (2010) 4758–4764.
[7] A. Nuttin, D. Heuer, A. Billebaud, R. Brissot, C. Le Brun, E. Liatard, J.M. Loiseaux, L. Mathieu, O. Meplan, E. Merle-Lucotte, H. Nifenecker, F. Perdu, S. David, Prog. Nucl. En. 46 (2005) 77–99.
[8] L. Mathieu, D. Heuer, R. Brissot, C. Garzenne, C. Le Brun, D. Lecarpentier, E. Liatard, J.M. Loiseaux, O. Meplan, E. Merle-Lucotte, A. Nuttin, E. Walle, J. Wilson, Prog. Nucl. En. 48 (2006) 664–679.
[9] N. Tyagi, A.A. Reddy, R. Nagarajan, Opt. Mater. 33 (2010) 42–47.
[10] A. Sarakovskis, J. Grube, A. Mishnev, M. Spingis, Opt. Mater. 31 (2009) 1517–1524.
[11] N.I. Sorokin, B.P. Sobolev, Crystallo Reports 52 (2007) 842–863.
[12] B. Gilbert, G. Mamantov, G.M. Begun, J. Chem. Phys. 62 (1975) 950–955.
[13] G.N. Papatheodorou, V. Dracopoulos, Chem. Phys. Lett. 241 (1995) 345–350.
[14] V. Dracopoulos, J. Vagelatos, G.N. Papatheodorou, J. Chem. Soc. Dalton Trans. (2001) 1117–1122.
[15] A.-L. Rollet, S. Godier, C. Bessada, Phys. Chem. Chem. Phys. 10 (2008) 3222–3228.
[16] A.-L. Rollet, C. Bessada, A. Rakhmatullin, Y. Auger, P. Melin, C. R. Chimie 7 (2004) 1135–1140.
[17] A.-L. Rollet, C. Bessada, Y. Auger, P. Melin, M. Gailhanou, D. Thaudière, Nucl. Instrum. Meth. Phys. Res. B 226 (2004) 447–452.
[18] A.-L. Rollet, A. Rakhmatullin, C. Bessada, Int. J. Thermophys. 26 (2005) 1115–1126.
[19] C. Bessada, A. Rakhmatullin, A.-L. Rollet, D. Zanghi, J. Nucl. Mater. 360 (1) (2007) 43–48.
[20] S. Watanabe, H. Matsuura, H. Akatsuka, Y. Okamoto, P. Madden, J. Nucl. Mater. 344 (1–3) (2005) 104–108.
[21] S. Watanabe, A. Adya, Y. Okamoto, N. Umesaki, T. Honma, H. Deguchi, M. Horiuchi, T. Yamamoto, S. Nogushi, K. Takase, A. Kajinami, T. Sakamoto, M. Hatcho, N. Kitamura, H. Akatsuka, H. Matsuura, J. Alloys Compd. 408–412 (2006) 71–75.
[22] A.-L. Rollet, V. Sarou-Kanian, C. Bessada, C. R. Chimie 13 (2010) 399–404.
[23] A.-L. Rollet, V. Sarou-Kanian, C. Bessada, Inorg. Chem. 48 (2009) 10972–10975.
[24] V. Sarou-Kanian, A.-L. Rollet, M. Salanne, C. Simon, C. Bessada, P.A. Madden, Phys. Chem. Chem. Phys. 11 (2009) 11501–11506.
[25] G.J. Janz, J. Phys. Chem. Ref. Data 17 (2) (1988) 1–309.
[26] J. Hives, J. Thonstad, Electrochim. Acta 49 (28) (2004) 5111–5114.
[27] M. Wilson, P.A. Madden, J. Phys.: Condens. Matter 5 (1993) 2687–2706.
[28] M. Salanne, C. Simon, P. Turq, P.A. Madden, J. Fluorine Chem. 130 (2009) 38–44.
[29] M. Salanne, C. Simon, H. Groult, F. Lantelme, T. Goto, A. Barhoun, J. Fluorine Chem. 130 (2009) 61–66.
[30] O. Pauvert, D. Zanghi, M. Salanne, C. Simon, A. Rakhmatullin, H. Matsuura, Y. Okamoto, F. Vivet, C. Bessada, J. Phys. Chem. B 114 (2010) 6472–6479.
[31] C. Bessada, A. Rakhmatullin, A.-L. Rollet, D. Zanghi, J. Fluorine Chem. 130 (2009) 45–52.
[32] G.N. Papatheodorou, J. Chem. Phys. 66 (1977) 2893–2900.
[33] C. Bessada, A.-L. Rollet, A. Rakhmatullin, I. Nuta, P. Florian, D. Massiot, C. R. Chimie 9 (2006) 374–380.
[34] G.M. Photiadis, G.N. Papatheodorou, J. Chem. Soc. Dalton Trans. 6 (1998) 981–989.
[35] G.M. Photiadis, G.N. Papatheodorou, J. Chem. Soc. Dalton Trans. 20 (1999) 3541–3548.
[36] P.A. Madden, M. Wilson, Chem. Soc. Rev. 25 (1996) 339–350.
[37] M. Salanne, C. Simon, P. Turq, P.A. Madden, J. Phys. Chem. B 112 (2008) 1177–1183.
[38] S. Nosé, Mol. Phys. 52 (1984) 255–268.
[39] G. Martyna, M. Klein, M. Tuckerman, J. Chem. Phys. 97 (1992) 2635–2643.